Titre: Title:	The Dual-Role of Benzothiadiazole Fluorophores for Enabling Electrofluorochromic and Electrochromic Devices
Auteurs: Authors:	A. Mohan Raj, Chengzhang Yao, Gokul Balakrishnan Muthuperumal, Lei Hu, Alexandre Malinge, Mathieu Frémont, Coralie Cambe, Orlando Ortiz Rodriguez, Sacha Porlier, & William G. Skene
Date:	2024
Type:	Article de revue / Article
Référence: Citation:	Raj, A. M., Yao, C., Muthuperumal, G. B., Hu, L., Malinge, A., Frémont, M., Cambe, C., Ortiz Rodriguez, O., Porlier, S., & Skene, W. G. (2024). The Dual-Role of Benzothiadiazole Fluorophores for Enabling Electrofluorochromic and Electrochromic Devices. ChemPlusChem, 28 pages. https://doi.org/10.1002/cplu.202400667

ChemPlusChem

Research Article
doi.org/10.1002/cplu.202400667

Chemistry Europe
European Chemical Societies Publishing

www.chempluschem.org

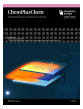

The Dual-Role of Benzothiadiazole Fluorophores for Enabling Electrofluorochromic and Electrochromic Devices

Mohan Raj Anthony Raj,[a] Chengzhang Yao,[a] Gokul Balakrishnan Muthuperumal,[a] Lei Hu,[a] Alexandre Malinge,[b] Mathieu Frémont,[a] Coralie Cambe,[a] Orlando Ortiz,[b] Sacha Porlier,[a] and W. G. Skene*[a, c]

Three unsymmetric fluorophores differing in their flanking electron acceptor (–NO_2, –CN, –CHO) were investigated for their electrofluorochromism and electrochromism. The emission yield of the -NO_2 substituted fluorophore in the solid state was ca. 9-fold less than its -CN and -CHO counterparts. Visible color changes of the fluorophores were observed with an applied potential. The intensity of the near-infrared absorption at ca. 1500 nm formed upon electrochemical oxidation was contingent on the electron-withdrawing group: 2-fold more intense with the -CN substitution than its -H counterpart. The coloration efficiency was upwards of 655 $cm^2 C^{-1}$ and the bleaching kinetics (t_b; 22 s) of the NIR band decreased according to -NO_2 > -CN > - CHO ≈ -H. The electrochemically generated states could be reversibly formed during 120 min of switching the applied potential. The contrast ratio of the radical cation and the NIR absorption was near unity and 60–82 %, respectively. The photoemission intensity of the fluorophores could also be modulated with applied potentials. The collective electrochemically mediated color switching and emission intensity modulation along with their solid-state emission demonstrate that benzothiadiazole fluorophores can play a dual role in chromic devices both as the color switching and photoemission intensity modulating material.

Introduction

Electrochemically mediated color changes enable light filtering coatings in smart windows.[1] Such an electrochromic use has a true ecological advantage. This is by reducing building cooling/heating loads by modulating the transmitted light that otherwise contributes to heat losses and gains.[2] The active component in these sustainable devices is typically a metal oxide, such as tungsten oxide.[3] The coating is robust and can undergo multiple cycles of attenuating reversibly the filtered light to meet the requirement for its long-term use in functional applications. An extended palette of colors spanning the visible spectrum and extending to the NIR is possible with their conjugated organic counterparts.[4] While conjugated polymers have been successfully used as the color switching material in electrochromic devices, they have played a limited role as a fluorophore in electrofluorochromic devices. These are devices whose photoemission intensity can be reversibly adjusted with an applied potential.[5]

The requisites of the active material for enabling both electrochromic and electrofluorochromic devices are visible color changes and photoemission intensity modulation with applied potential.[6] Appreciable emission yield (Φ_{fl}) when cast as a thin film along with reversible electroactivity are additional key properties that are required of fluorophores for them to be used as dual-role active layers. These are materials that can modulate their color and their photoemission intensity with applied potentials. Such active materials can enable the simultaneous functioning of combined devices: electrochromic and electrofluorochromic. Although conventional fluorophores meet the emission requirements in solution as an electrofluorochrome, their intrinsic fluorescence is quenched by various modes in the solid state. This precludes the use of intrinsic fluorophores as light-induced emitters in operating electrofluorochromic devices.

Benzothiadiazoles are ideal candidates for dual-role materials in chromic devices.[7] This is in part because of their absorption in the visible spectrum.[8] Access to colorful molecular benzothiadiazoles is possible by catalytic methods along the lines of their polymer counterparts.[9] The emissive wavelength of molecular benzothiadiazoles such as dyads and triads can be adjusted with both the type of aromatic and the electronic groups that are conjugated with a central heteroaromatic,[8a,10] co-assembled structures,[11] and polarity.[12] Most importantly, conjugated benzothiadiazoles behave as conventional fluorophores with high Φ_{fl} in solution.[13] In contrast to conventional fluorophores, the intrinsic emission of benzothiadiazoles can be carried over to the solid-state.[14] This

[a] M. R. A. Raj, C. Yao, G. Balakrishnan Muthuperumal, L. Hu, M. Frémont, C. Cambe, S. Porlier, W. G. Skene
Department of Chemistry, Université de Montréal, Montreal, QC, Canada H3C 3J7
E-mail: w.skene@umontreal.ca

[b] A. Malinge, O. Ortiz
Department of Engineering Physics, Polytechnique Montréal, Montreal, QC, Canada H3T 1J4

[c] W. G. Skene
Institut Courtois, Université de Montréal, Montreal, QC, Canada H3C 3J7

Supporting information for this article is available on the WWW under https://doi.org/10.1002/cplu.202400667

has been exploited for using benzothiadiazoles in various applications, including imaging,[15] electrochemiluminescent sensing,[16] solid-state lasers,[17] and emitting devices.[14a,18] However, benzothiadiazoles are intrinsically electrochemically inert within the working limits of solvents that are commonly used for the electrochemical measurements. The electroactivity that is required for their use in electrochromic applications is possible by covalently coupling an electroactive group to the intrinsic electron accepting benzothiadiazole. For example, a reversible oxidation is possible by the covalent attachment of triphenylamine to benzothiadiazoles.[19] The added benefit of the electroactive moiety is its electron donating property. The electroactive segment can undergo intramolecular charge transfer with an electron accepting group when the chromophore is irradiated, leading to detectable emission in the visible region.[12a,20] The emission wavelength of the resulting intramolecular charge transfer can be adjusted with the strength of the electron-withdrawing group.

The visible color, solid-state emission, and reversible electroactivity of benzothiadiazoles make them ideal dual-mode candidates for use in both electrochromic and electrofluorochromic devices. Despite these collective properties and the extended use of benzothiadiazole as functional materials, their dual role for enabling combined electrochromic and electrofluorochromic devices remains in its infancy.[21] More specifically, their electrochemically mediated photoemission intensity modulation and their use in electrofluorochromic devices is underexplored.[5b–d,22] Towards this end, the impact of electron acceptors of varying strength ($-NO_2$, -CN, and -CHO) on the electroactive fluorophores (Chart 1) as dual-role materials are herein evaluated. Of importance is the effect of the electron substitution on the near infrared absorption for the oxidized intermediate. This is a key requirement of smart windows for reversibly filtering the NIR solar spectrum on demand for reducing radiant heating of buildings.[23] Knowledge about the color and fluorescence intensity modulation performance is beneficial for designing materials that have well-defined electrochemically mediated properties for enabling both electrochromic and electrofluorochromic devices. Towards providing such knowledge, the solid-state and solution emission are herein presented and complemented with color switching and photoemission modulation with applied potentials. These serve to demonstrate that unsymmetric donor-benzothiadiazole-acceptor can play a dual role: both color switching and fluorescence modulation for enabling electrochromic and electrofluorochromic devices.

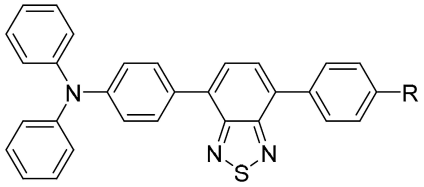

1 R=NO_2
2 R=CN
3 R=CHO
4 R=H

Chart 1. Benzothiadiazoles with electron-withdrawing groups of varying strength and its benchmark (R=H) prepared and investigated for their use as dual-role materials in chromic materials.

Results and Discussion

Spectroscopic Properties

The spectroscopic properties of **1–3** were investigated to assess their suitability as a dual-role fluorophore in a combined working electrochromic/electrofluorochromic device. To better evaluate the effect of the electron-withdrawing nitrile and nitro on the electronic *push-pull-pull* chromophores, the spectroscopic properties were compared to the known **3** with a withdrawing substituent of moderate strength.[18b] Moreover, establishing accurate emission wavelength and Φ_{fl} relationships with solvent polarity would be useful for tracking the polarity within an operating device (operando) and the potential change in polarity when functioning. Although various spectroscopic properties of **2** and **3** have been reported,[10a,18b] they were remeasured for benchmarking the properties of **1** and **2** under similar conditions. This was to accurately correlate the emission with polarity, required for assessing the polarity operando and the thin films. The solvatochromism and the solvent dependent Φ_{fl} of the three fluorophores with electron-withdrawing groups of varying strength can therefore be directly compared.

Both the solvent dependent absorption and emission spectra of the fluorophores were evaluated to assess their photoinduced intramolecular charge transfer.[24] According to Table 1, the absorption of **1** varies by 32 nm. **1** was sensitive to solvent polarity as illustrated by its negative solvatochromism (Figure S1). Both **2** and **3** similarly underwent a ca. 25 nm negative solvatochromism (Figures S2 and S3). The solvent dependent emission wavelength is more pronounced than the ground state solvent induced shifts. This is apparent when taking hexane as a benchmark for **1**, in which only the local excited state can be generated and not the charge transfer state. The emission of **1** shifted bathochromically upwards of 180 nm with increasing solvent polarity. The solvent induced spectroscopic perturbation is further evident with the Stokes shift, which was upwards of 10 000 cm^{-1}. The strength of the electron-withdrawing group affects the spectra. The donor also affects the charge transfer emission. This is apparent with the emission of **1** and **2** that is blue-shifted from their stronger *N*,*N*-dimethylamine donor counterparts.[12a] This aside, the perceived color of the emission was green in apolar solvents and it shifted towards the near-infrared region with increasing solvent polarity (Figure 1 and inset).

The solvatochromic behavior of the three fluorophores was consistent (Figures S4 and S5), albeit more pronounced for **1** than for **2** and **3** (Table 1). The similar shifts of **2** and **3** imply that the electron-withdrawing strength of the terminal group is similar for the two fluorophores. This is supported by the calculated dipole difference between the ground and excited

Table 1. Selected photophysical properties of the fluorochromes in various solvents.

	1				2				3			
Solvent	λ_{abs} (nm)[a]	λ_{em} (nm)[b]	Φ_{fl} (%)[c]	Stokes shift[d] (cm^{-1})	λ_{abs} (nm)[a]	λ_{em} (nm)[b]	Φ_{fl} (%)[c]	Stokes shift[d] (cm^{-1})	λ_{abs} (nm)[a]	λ_{em} (nm)[b]	Φ_{fl} (%)[c]	Stokes shift[d] (cm^{-1})
Hexane	456	548	91	3800	450	542	90	5000	450	540	94	3700
Toluene	455	600	87	5400	451	591	80	5700	452	590	95	5200
Acetone	443	730	0.9[e]	9400	432	732	20	11 000	438	707	17	9000
Diethyl ether	447	625	83	6700	447	608	85	6200	444	606	77	6000
THF	452	678	40	8000	444	658	71	8000	445	654	63	7200
Dichloromethane	457	672	1.5[e]	9000	446	672	65	8100	445	673	63	7600
Chloroform	465	660	3.5[e]	7100	452	654	70	7200	453	642	74	6500
Acetonitrile	440	700	0.2[e]	10 000	432	732	7	10 000	428	743	4	9900
Ethyl acetate	443	672	44	9600	427	650	65	8500	435	650	60	7600
Methanol	433	660	0.3 0.9[e]	7700	439	696	0.2[e]	9500	429	710	1	9200
DMSO	455	712	0.1[e]	9000	428	740	4[e]	10 500	443	750	3	9250
Solid state[h]	490	675	6	5750	445	625 (610)[i]	50 (60)[i]	5700	460	640 (638)[j]	54 (54)[j]	6030

[a] Maximum absorbance at longest wavelength. [b] Maximum emission at longest wavelength. [c] Absolute quantum yields measured with an integrating sphere. [d] Conversion from nm to cm^{-1} and corrected for λ^2. [e] Quantum yield relative to ruthenium tris(bipyridine) dichloride (Φ_{fl} = 2.8% in water).[18b,28] [h] Φ_{fl} measured with an integrating sphere as a thin film on glass slides. [i] Value in parentheses from literature as-prepared powder.[10a] [j] Value in parentheses from literature as thin film.[18b]

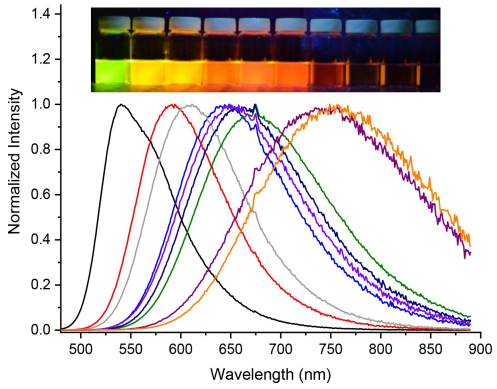

Figure 1. Normalized emission spectra of **2** in hexane (black), toluene (red), chloroform (blue), diethyl ether (gray), dichloromethane (green), tetrahydrofuran (navy blue), ethyl acetate (purple), acetonitrile (wine), and DMSO (orange) photoexcited at the most red-shifted absorbance. Inset: photograph of vials of **1** irradiated with a handheld UV lamp at 365 nm in hexane, toluene, chloroform, diethyl ether, dichloromethane, ethyl acetate, THF, acetonitrile, and DMSO (left to right).

states, being 17.7 D for **1**. In contrast, the dipole differences for **2** and **3** were smaller, 14.5 and 14.2 D, respectively. These values were consistent with the Lippert-Mataga derived dipole (15 D; Figure S10).[25] The strength of the electron-withdrawing group can be ranked in increasing order according to **3**, **2**, and **1** according to the dipoles. The large dipole difference can be ascribed to the coplanarization of the central conjugated aromatics. Indeed, the calculated dihedral angles of the substituted phenyl and the triphenyl with the central benzothiadiazole decreased, on average, by 21.6 and 28°, respectively, in the excited stage relative to their corresponding optimized ground state geometries.

It is worthy to establish that the polarity of dichloromethane resembles the environment of both the electrofluorochromic electrolyte and a working solid-state electrochromic device. Therefore, the emission of dichloromethane could be used to predict the emission and the Φ_{fl} in electrofluorochromic devices (vide infra). The photoemission of the three fluorophores was consistent in dichloromethane and their emission was at the cusp of the visible spectrum and it extending to the NIR. There was no perceived difference between the various fluorophores. The Φ_{fl} of **2** and **3** in dichloromethane with the supporting electrolyte used for the spectroelectrochromic and electrofluorochromic measurements was also consistent with the values measured in neat dichloromethane. This confirms the supporting electrolyte is spectroscopically innocuous even at the high concentrations required to make the organic solvent conductive. This, taken together with the consistent intrinsic fluorescence when coated as a thin layer on transparent substrates (Table 1), prove the fluorophores are ideal for solid-state applications such as electrofluorochromic devices.

The temperature dependent emission was also evaluated to further assess the effect of the electron withdrawing group on the emission. The emission of the three fluorophores red shifted with decreasing temperature (87 nm; Figures S7-S9). The observed shifts are consistent with increasing stability of the excited state with decreasing temperature. This can arise by the lowest energy conformation being preferentially formed in the excited state by coplanarizing the terminal phenyls with the benzothiadiazole core. This enhances intramolecular charge transfer and subsequent photoemission from this state rather than the local excited state.[27] The emission intensity also decreased upon lowering the temperature. The emission of **2** and **3** decreased ca. two-fold at low temperature when not taking the temperature dependent refractive index variation of the solvent into account. The effect was more pronounced with **1**, whose emission decreased fourfold at low temperature. The emission quenching at low temperature is likely from non-

radiative deactivation such as vibronic coupling of the HOMO and LUMO energy levels.

Key properties the fluorophores must possess for them to be used in working combined electrochromic and electrofluorochromic devices are: 1) visible color changes, 2) emission in the visible region, 3) appreciable Φ_{fl} in the solid state, 4) reversible redox activity, and 5) reversible color change and photoemission intensity modulation with applied potential. Given the pronounced solvatochromic effect of the fluorophores, their solvent dependent Φ_{fl} was investigated. This was to ensure the fluorophores maintained their emission under conditions that mimicked an operating device. As expected, the Φ_{fl} of **1** was affected by solvent polarity.[29] The values ranged from near unity ($\Phi_{Fl}=91\%$; Table 1) in hexane, with the exclusive formation of the local excited state, to essentially being quenched (1%) in methanol.

The Φ_{fl} in dichloromethane, chloroform, and THF is of interest. This is because these solvents are commonly used for electrochemical measurements, especially electrofluorescence. Appreciable emission in these solvents is desired for monitoring the electrochemically mediated changes in fluorescence intensity. In the cases of **2** and **3**, their high degree of fluorescence was preserved. In contrast, **1** appreciably fluoresced in only THF. The fluorophores nonetheless emit in solvents that are used for electrochemically mediated fluorescence quenching, allowing their electrofluorochromic behavior to be evaluated. The persistent emission was also evaluated in the electrolyte solution commonly used for assessing electrofluorochromism: dichloromethane with tetrabutylammonium perchlorate. The Φ_{fl} of both **2** and **3** in the electrolyte was consistent with their corresponding Φ_{fl} in neat dichloromethane. As such, both fluorophores were expected to be ideally suited for electrofluorochromic devices.

While a high Φ_{fl} is an ideal property for using the fluorophores in electrofluorochromic devices, the emission behavior in solution does not necessarily carry over to the solid-state. Solid-state emission is a key requirement for the fluorophore to be used as an active layer in solid-state electrofluorochromic devices. This is possible with fluorophores that undergo aggregation induced emission (AIE).[30] Such is the case with most conjugated benzothiadiazoles.[14b,31] Both **2** and **3** were emissive in the solid state (Table 1) along with operating devices and they were insensitive to oxygen. Both **2** and **3** emitted appreciably in the solid state. In contrast, the emission of **1** was an order of magnitude less than its counterparts. The solid-state emission of **2** and **3** confirmed the two fluorophores have ideal properties for their use as active layers in electrofluorochromic devices. In contrast, the muted solid-state emission of **1** was expected to result in reduced device performance compared to its highly emissive counterparts.[32]

Electrochromism

Reversible oxidation is required of the fluorophores for their electrochromic use. The redox potentials of the three fluorophores were both consistent and reversible according to cyclic voltammetry.[33] This was expected, since oxidation occurs on the common triphenylamine segment of the fluorophores. Only one oxidation process was observed (Figure S11) and it was consistent ca. 540 mV vs. Fc/Fc^+ for the three fluorophores. The oxidation potential of **1** and **2** was ca. 70 mV more positive compared with their counterpart whose triarylamine is replaced with -NMe_2. This is owing to the weaker donor of the triarylamine amine relative to the aliphatic amine.[12a] The one-electron oxidation process was reversible. Both similar electrochemical reversibility and the oxidation potential were found for **3**, being consistent with those previously reported.[18b]

A critical property that materials must possess for their use as an active layer in electrochromic devices is a reversible change in color with applied potential, especially in the NIR region. This can be evaluated spectroelectrochemically. As expected, the absorption of the neutral fluorophores bleached with applied potential along with the color changes from orange to dark blue. The absorption in the blue region of the visible spectrum (450 nm, $\varepsilon = 16\ 100 \pm 400\ M^{-1}\,cm^{-1}$), corresponding to the neutral state, was replaced with three broad absorptions: a weak one between 536 and 600 nm, another more intense centered at ca. 860 nm, and a third at the onset of the NIR at 900 nm that extended outwards to 2200 nm. The two absorptions in the visible and the cusp for the NIR are characteristic of the radical cation. A target criterion of the fluorophores for use in smart window applications is abroad absorption in the NIR to reduce radiant heating. This is of importance because the NIR absorption change with applied potential for the *N*,*N*-dimethylamino counterparts of **1** and **2** have not been explored. The fluorophores met this metric because of their broad NIR absorption in the 900 to the 2000 nm region upon oxidation.[21]

The desired NIR absorption formed concurrently with the radical cation upon electrochemical oxidation of the three fluorophores (Figure 2). The conversion of the neutral state to the charged intermediate was concluded by the isosbestic point at ca 415 nm (Figures S13A and S17 A). The charge transfer band decreased and it was replaced entirely by the absorption of the radical cation with increasing potential. The absorbance of the radial cation depleted completely when it was neutralized by decreasing the applied potential. The absorption of the original neutral state was restored once the oxidized state had been depleted.

The electronic group played an important role in the absorptions upon oxidization. In the case of **1**, the NIR absorption increased in intensity with applied potential (ca. $\varepsilon = 2\ 000\ M^{-1}\,cm^{-1}$; Table S1), centered at 1480 nm. The NIR absorption of **2** was red shifted by 20 nm relative to **1** with a ca. 40% increase in its calculated ε. This contrasts with **3** with the weaker electron acceptor whose absorption was blue shifted by 40 nm compared to **1** along with a 4% reduction in intensity. To confirm the effect of the electronic groups on the NIR charge transfer absorption and its intensity, the benchmark **4** without an electron-withdrawing group was investigated. Indeed, its NIR absorption was two-fold less (Figure S21) than the other three fluorophores.

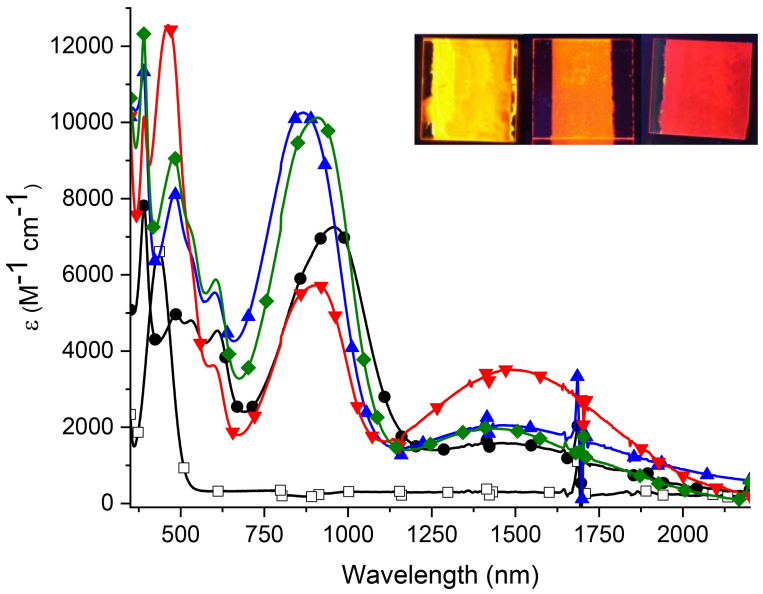

Figure 2. Absorption spectra of the neutral (open symbols) and electrochemically oxidized (closed symbols) states of **1** (blue), **2** (red), **3** (green), and **4** (black) measured with a honeycomb electrode. Insert: photographs of **1**–**3** deposited on glass substrates and irradiated with the handheld UV lamp.

The absorption of $\mathbf{1}^{\bullet+}$ in the visible region was as broad as **2** and it was centered at 608 nm (8150 $cm^{-1}M^{-1}$). Its absorption was at 853 nm (18 100 M^{-1} cm^{-1}; Figure 2). An absorption at 616 nm (10 250 M^{-1} cm^{-1}) was observed for **3** along with an absorption in the NIR region at 865 nm (21 900 M^{-1} cm^{-1}). In all cases, the absorption $<$ 855 nm increased with increasing time the potential was applied. The electrochemically induced absorptions in this region were more intense than their corresponding changes in the visible region. The color of the fluorophores' neutral state bleached with increasing the time the potential was applied, resulting in a perceived visible-to-invisible color change. The fluorophores therefore act as visible switches with color changes in the visible and NIR regions that are contingent on the strength of the terminal electronic withdrawing group. The collective spectral changes in both the visible and broadband NIR are ideal for using the fluorophores in smart windows.

Theoretical calculations were done to complement the spectroelectrochemical studies and to further understand the effect of the electronic withdrawing groups on the absorption spectra. For this, dichloromethane was chosen as a solvent continuum to mimic the spectroelectrochemical conditions. Similar to the dipole moments (vide supra), the absolute electronic transitions cannot be accurately calculated. However, the trend between the series of compounds that are calculated in the similar way can be derived.

The calculations helped visualize the spin density of the radical that was concentrated on the triarylamine. It also extended out to part of the adjacent benzothiadiazole (Figure S23). Subtle differences in the electronic transitions were also calculated for the three compounds. For example, the most red-shifted absorption of the neutral state varied by only 9 nm between the three fluorophores. While both **2** and **3** had similar electronic absorptions, **1** was the most red shifted. This was expected because of its stronger electron withdrawn substituent. Specifically, the absorption was centered at 405, 397, 400, and 390 nm for **1**, **2**, **3**, and **4**, respectively (Figure S25). The absorption of the radical cation was red shifted for each fluorophore relative to its corresponding neutral state as expected. The calculated trend was consistent with the spectroelectrochemical measurements. While there is little difference in the absorptions between the three fluorophores, the relative difference between their respective neutral and radical cation states is unique. The difference increased according to the order of **4**, **3**, **1**, and **2**. Of noteworthiness are the calculated oscillator strengths for the lowest energy electronic transitions of the neutral that were double that of the charged intermediates of the three fluorophores.

The natural transition orbitals (NTO) were also calculated to visualize the principal molecular orbitals involved in the lowest electronic transition of the given state. The highest occupied orbital with the highest occupancy was located on the triphenylamine segment and it extended slightly out to the phenyl of the acceptor terminus (Figure S24). The absorptions of the electrochemical oxidized fluorophores in the visible and in the NIR regions are significantly different than those of the corresponding neutral state. This visible spectroscopic change makes the fluorophores useful as electrochromes. While the calculations cannot capture the NIR charge transfer, they do confirm the vertical transitions of both the neutral state and the radical cation occur in the visible region. The broad NIR absorption measured by spectroelectrochemistry can be assigned to a charge transfer with the open shell charged species based on known experimental observations of similar systems.[34]

The spectroelectrochemical measurements confirmed the fluorophores were both electroactive and they changed colors with applied potential. Insight into the colorfastness of the

fluorophores, notably their capacity to sustain repeated color switching over extended periods, was evaluated by monitoring their change in transmission % at a given wavelength when switching the applied potentials between the neutral and oxidized states over many cycles. The NIR absorption at 850 nm was chosen to examine the colorfast of the oxidized intermediate. All of the compounds could be switched between their neutral and oxidized states for up to 2 hours with switching the applied potential at 2 min intervals. During these periods, the transmission % of the respective state could be reversibly regenerated (Figure 3A, S13B and S17B). The materials can therefore sustain multiple switching between the two states without degrading. This metric confirms their suitability as electroactive layers in operating electrochromic devices, especially smart windows.

Another important performance criteria that must be met to use the fluorophores in optical applications is the contrast ratio. A near-unity contrast ratio (>92%; Figure 3A and Table 2) was measured between the neutral state and radical cation for the three fluorophores at identical concentrations. The contrast ratio for the corresponding NIR absorption was somewhat muted, between 61 and 82%. The highest contrast ratio for both electrochemically induced intermediates was observed for **2**. The $R^{\bullet+}$ state took ca. 22 sec to reach 90% change in transmission and it took twice as long to bleach to the original state (Figures S13C, and S17 C).[35] The $R^{\bullet+}$ coloration kinetics were 21–24 sec for the NIR absorption for **1**–**3** and they were independent of the electron substitution. The bleaching rate (t_b) of the oxidized state was affected by the electron-withdrawing group. Taking **4** as the benchmark, the bleaching rate increased proportionally with the strength of the electron-withdrawing group. The intrinsic t_b of **3** was similar to **4** in the absence of applied potential. This contrasted with the t_b for **2** and **1** that were 1.5-fold and two-fold faster than **4**, respectively (Figure S12).

It is worthy to note that the performance data, such as coloration/bleaching kinetics and coloration efficiency, are unknown for benzothiadiazole electrochromes. The exception is the triphenylamine-benzothiadiazole-*N*,*N*-dimethylamine counterpart of the fluorophores.[36] The switching times of this unsymmetric electronic *push-pull-push* counterpart were 12 and 80 sec for the coloration (t_c) and the bleaching times, respectively. Accordingly, the electron-withdrawing group accelerates the t_b, yet slows the t_c. Nonetheless, the measured kinetics were consistent with other molecular electrochromes.[37] The switching kinetics of the polymer counterparts of the fluorophores are faster. This is because the kinetics are limited by the electron transfer process in thin films.[33] This contrasts with the measurements of **1**–**4** in solution whose switching kinetics are limited by mass transfer to the electrode. Direct comparison of immobilized films and solution is therefore not possible. The bleaching kinetics can nonetheless be accelerated by increasing the strength of the electronic acceptor. Therefore, integrating multiple electron withdrawn groups in the conjugated scaffold has the potential to significantly accelerate the beaching kinetics. This would overcome the current challenge of device kinetics, opening other areas of electrochromic use other than smart windows. Bearing this in mind, the coloration kinetics of the dual-mode materials fall within the range for use as smart coatings. The coloration times of the fluorophores

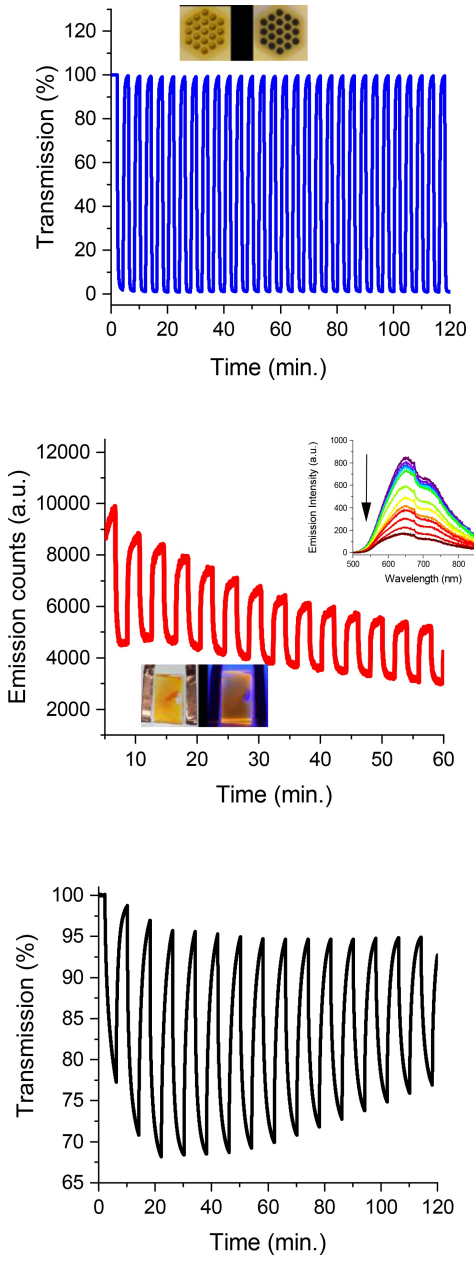

Figure 3. A) Transmission percent change of **2** in anhydrous and degassed dichloromethane monitored at 850 nm with applied potentials between +0.6 and −0.5 V vs. Au reference electrode switched at 2 min intervals. Inset: photograph of the honeycomb electrode for the neutral (left) and oxidized (right) states of **2**. B) Change in emission intensity of the operating electrofluorochromic device prepared with **2** as the active layer with applied potentials switching between +1.8 and −0.5 V excited at 450 nm and monitored at 620 nm. Inset: change in fluorescence of **2** in dichloromethane with $TBAClO_4$ (0.1 M) excited at 450 nm with applied potentials from 0.5 V to 2.2 V vs. Ag° pseudo-reference electrode (top) and electrofluorochromic device of **2** irradiated under ambient light (left) and with a UV handheld lamp at 365 nm. C) Change in transmittance percent of an operating electrochromic device prepared from **2** monitored at 800 nm with potentials between 2.2 V and −0.5 V at 2 minute intervals.

Table 2. Performance of fluorophores in solution and in combined operating electrochromic and electrofluorochromic devices.

Compound	η (cm^2 C^{-1})	Transmission % difference (800–850) nm	Contrast ratio (%) (800–850) nm	(1430–1500) nm	Fluorescence[a]
1	352	100	92	61	47
2	623	100	96	82	49
3	656	100	95	57	50
Device 2[b]	100	26	28	–	44
Device 3[b]	266	48	47	–	26

[a] Averaged over the three complete periods; λ_{ex} = 450 nm; λ_{em} = (620 - 680) nm. [b] Operating electrochromic/electrofluorochromic device using the corresponding fluorophore as the active layer.

would be accelerated when immobilized as a thin film on the electrode.

The performance of the fluorophores was further benchmarked by measuring their coloration efficiency (η). The linearly derived η was 352, 623, and 652 cm^2 C^{-1} for **1**, **2** and **3**, respectively (Figure S22). The coloration efficiencies are comparable to reported amino substituted triphenylamine electrochromes, demonstrating the conjugated electronic *push-pull* maintains the desired coloration efficiency.[39] The η was consistent for the moderate strength electron-withdrawing groups. Indeed, the same amount of charge was required to induce the targeted 100% change in optical transmission for **2** and **3**. In contrast, more charge was required to induce the color change with the strong withdrawing nitro. This is according to the lower η of **1** relative to **2** and **3**. Nonetheless, the measured η of **1**–**3** is consistent with known molecular electrochromes although the coloration kinetics are on par with molecular electrochromes,[37] albeit tenfold slower than polymer films in part because of diffusion kinetics.[6a]

Working devices of **1**–**3** were fabricated to test the true potential of the fluorophores as dual-role materials in operating devices. The performance of **1**–**3** was benchmarked against their similar properties measured in solution. The change in absorption of **2** and **3** in the device was consistent with the spectroelectrochemical measurements (Figures S15 and S19). This confirms the polymer gel and the electrolyte do not affect the spectroscopic properties in the solid-state device. However, the perceived color of the oxidized state was green owing to the predominate absorption at ca. 800 nm. The contrast ratio of **2** and **3** in operating devices was reduced by two thirds and more than half, respectively. Although the performance of **2** and **3** in operating devices is maintained compared to their spectroelectrochemical measurements (Figure 3C and S19), their color changing kinetics remained low compared to other molecular electrochromes. The η in operating devices was also reduced compared to the solution measurements (Table 2). In this case, more current was required to change the color along with a reduced contrast ratio. This is ascribed to the increased resistance of the electrolyte polymer along with the fluorophore film on the electrode compared to the highly conductive electrolyte solution in which **1**–**3** were more dilute.

Electrofluorochromism

The modulation of the fluorescence intensity with applied potential upon irradiation was also examined to assess the suitability of the fluorophores as dual-role materials; capable of both reversible color switching and fluorescence intensity quenching with applied potential. The emission spectra were first measured to see the effect of the supporting electrolyte on the emission relative to pristine dichloromethane (vide supra). The measured emission maximum was 680 nm for both **2** and **3** and 670 nm for **1**. Only in the cases of **1** and **2** was the emission red shifted by 10 nm, relative to pristine dichloromethane (Figure S16). This implies that the perceived polarity of the electrolytic solution by these two fluorophores is marginally more polar than pristine dichloromethane. The emission shifts further demonstrate the type of electron withdrawing group that is conjugated to the benzothiadiazole senses its environment and it alters its emission wavelength accordingly. Although the fluorescence of **1** was significantly less than **2** in dichloromethane, it nonetheless fluoresced in a sufficient amount to assess its photoemission intensity modulation with applied potential. The electrochemically mediated change in fluorescence intensity is evident in Figure 3B for **2** where the emission is reduced appreciably when the oxidized state is formed. Indeed, the fluorescence contrast ratio was reduced by half compared to the color contrast ratio.

The electrochemically quenched fluorescence could be regenerated by reducing the oxidized intermediate to the neutral state. It is worthy to note that the radical cation was recently confirmed to emit albeit in an unknown amount.[21] The residual emission that was observed after applying the positive potential for a given period of time cannot be unequivocally assigned to this transient. This is because of a mismatch between the surface area of the working and counter electrodes. This is exacerbated by diffusional effects in the cuvette. The neutral fluorophore can continuously diffuse to the working electrode during the measurements and replenish the oxidized fluorophore, resulting in no perceived reduction in emission intensity. This aside, the intrinsic emission of the fluorophores can be reversibly modulated electrochemically during 5 min. intervals of switching the potential (Figure 3B).

Working devices were fabricated to further investigate the fluorescence intensity modulation with applied potential upon

photoexcitation. The emission maximum of the devices was blue shifted (636 ± 10 nm) compared to their emission in neat dichloromethane (675 ± 10 nm) (Figure S16). This shift was due to the change in the polarity in the device as well as from restricted motion. The absolute emission yield of the device was benchmarked to assess the effect of the different components on quenching the fluorophore's emission. In the case of **1**, there was little effect and the device Φ_{fl} (2.2%) was consistent with pristine dichloromethane (Φ_{fl} = 2%; Table 1). In contrast, the emission of **2** and **3** in the device decreased by 2.8-fold and 7.7-fold (Figures 3 inset and S20 A), respectively, compared to pristine films of the fluorophores on glass.

Similar to what was observed for electrofluorochromic measurements in solution, the emission intensity of the fluorophores in the operating device was reversible when switching the applied potentials between the neutral and oxidized states (Figures 3B and S20B). The devices were operated for 30 minutes. Afterwards the Φ_{fl} was remeasured. The value before and after switching decreased to 12% and 23% for **2** and **3**, respectively. The fluorescence contrast ratio of the device of **2** was nonetheless consistent with the value measured in solution (Table 2). Conversely, the contrast ratio of **3** in a device reduced by half compared to measurements done in solution. The working devices demonstrate the intrinsic fluorescence of the fluorophore can be preserved when the fluorophore is used as an electroactive layer in a device. Their fluorescence intensity can also be reversibly switched electrochemically. The overall decrease in the absolute fluorescence intensity during device operation is most likely a result of irreversible migration of the fluorophore towards the cathode, resulting in memory effects. The results nonetheless demonstrate the dual-role use of the fluorophores in operating devices: color switching and fluorescence intensity modulation. Moreover, the fluorophores have the requisite intrinsic properties for use in combined electrochromic and electrofluorochromic devices. The device performance can be improved by optimizing the fabrication to include coating and electrolyte thickness along with electrolyte composition.

Conclusions

The strength of the electron-withdrawing group had pronounced effects on the spectroscopic, electrochromic, and electrofluorochromic properties. Subtitle changes in the strength of the withdrawing group and the solvent impact the emission yield. Ultimately, their sensor-like properties can report the polarity *operando* of working electrochromic devices. The electron-withdrawing group promotes the NIR absorbance with an applied potential whose wavelength and intensity were contingent on the strength of the acceptor. Overall, the nitrile acceptor provided the best electrochromic and electrofluorochromic performance in both solution and operating devices. The device performance, specifically the consistent off/on photoemission intensity of the fluorophores, can potentially be improved by immobilizing the chromophore on the anode. Meanwhile, tuning the color and both the emission wavelength and the solid-state emission of benzothiadiazoles make them ideal dual-mode materials for use in combined electrochromic and electrofluorochromic devices. The dual role of the fluorophores was demonstrated by their collective change in absorption and photoemission intensity with applied potential. The use of the materials in devices is further spurred on by their high coloration efficiency. Ultimately, devices emitting across the visible spectrum that are capable of electrochemically mediating the photoemission intensity modulation are possible by tuning the functional group that is conjugated with the benzothiadiazole core and the triphenylamine terminus.

Experimental

Synthesis

4-(7-Bromobenzo[c][1,2,5]thiadiazol-4-yl)-*N*,*N*-diphenylaniline (**1 a**).[40] 4,7-Dibromobenzo[c][1,2,5]thiadiazole (2.00 g, 6.8 mmol) and 4-(diphenylamino)- phenyl boronic acid (1.97 g, 6.8 mmol) were dissolved in THF (50 mL) and a solution of potassium carbonate (2 M, 10.2 mL) was then added to the mixture. A catalytic amount of $Pd(PPh_3)_4$ was added to the mixture under an argon atmosphere. The mixture was heated to 80 °C and stirred for 8 h under argon. After cooling to room temperature, the mixture was washed with water and it was extracted with dichloromethane. The crude product was purified by silica gel column chromatography with dichloromethane/hexane (v/v = 1:6) as eluent. The title compound was obtained as an orange solid (2.5 g, 68%).^{1}H NMR (400 MHz, $CDCl_3$) δ 7.93 (d, *J* = 7.6 Hz, 1H), 7.84 (d, *J* = 8.8 Hz, 2H), 7.58 (d, *J* = 7.6 Hz, 1H), 7.38 – 7.30 (m, 4H), 7.26 – 7.19 (m, 6H), 7.11 (t, *J* = 7.3 Hz, 2H). ^{13}C NMR ($CDCl_3$, 100 MHz) δ ppm = 154.1, 153.3, 148.6, 147.5, 133.7, 132.5, 130.1, 130, 129.6, 127.5, 125.2, 123.6, 122.7, 112.3. ESI-MS [M + H$^+$]: m/z calcd for $C_{24}H_{16}BrN_3S$ 458.4, found 458.1.

4-(7-(4-Nitrophenyl)benzo[c][1,2,5]thiadiazol-4-yl)-*N*,*N*-diphenylaniline (**1**). **1 a** (1.0 g, 2.2 mmol, 1.0 eq), sodium carbonate (463 mg, 4.4 mmol, 2.0 eq), 4-nitrophenylboronic acid (364 mg, 2.2 mmol 1.0 eq), were added in a dry 250 mL two-neck round bottom flask under nitrogen. Then anhydrous toluene:ethanol:water (40:10:5 mL) was added to the flask. The solution was purged with nitrogen for 20 minutes. Then, tetrakis(triphenylphosphine)palladium (150 mg, 0.12 mmol, 0.05 eq) was added to the solution. The reaction mixture was next heated to reflux for overnight under a nitrogen atmosphere. Upon cooling, the mixture was diluted with dichloromethane. The organic phase was washed with water and then extracted. It was dried over magnesium sulfate, filtered, and then concentrated. The crude product was purified over silica gel (hexane/dichloromethane; 60:40) to afford the product as a violet solid (640 mg, 59%). ^{1}H NMR (400 MHz, $CDCl_3$) δ 8.43 (d, *J* = 8.9 Hz, 2 H), 8.22 (d, *J* = 8.9 Hz, 2H), 7.92 (dd, *J* = 11.4, 8.1 Hz, 3H), 7.84 (d, *J* = 7.4 Hz, 1H), 7.38 – 7.31 (m, 4H), 7.24 (t, *J* = 7.7 Hz, 6H), 7.12 (t, *J* = 7.3 Hz, 2H).^{13}C NMR ($CDCl_3$, 100 MHz) δ ppm = 154.15, 153.8, 148.65, 147.5, 147.4, 143,9, 138.35, 134.8, 130.2, 130.0, 129.9, 129.55, 129.4, 128.45, 127.0, 125.2, 123.7, 122.6. ESI-MS [M + H$^+$]: m/z calcd for $C_{30}H_{20}N_4O_2S$ 500.6, found 501.2.

4-(7-(4-(Diphenylamino)phenyl)benzo[c][1,2,5]thiadiazol-4-yl)benzonitrile (**2**).[10a] Synthesized following a similar procedure to **1** with **1 a** (1.0 g, 2.2 mmol, 1.0 eq), sodium carbonate (463 mg, 4.4 mmol, 2.0 eq), 4-cyanophenylboronic acid (385 mg, 2.62 mmol, 1.2 eq), and tetrakis(triphenylphosphine)palladium (126 mg, 0.11 mmol, 0.05 eq). The product was purified over silica gel

(hexane/dichloromethane; 50:50) to afford an orange solid (970 mg, 89%). ^{1}H NMR (400 MHz, $CDCl_3$) δ 8.15 (d, J=8.6 Hz, 2H), 7.92 (d, J=8.8 Hz, 2H), 7.88 – 7.80 (m, 4H), 7.37 – 7.31 (m, 4H), 7.25 (dt, J=8.6, 4.9 Hz, 6H), 7.12 (t, J=7.3 Hz, 2H). ^{13}C NMR ($CDCl_3$, 100 MHz) δ ppm=154.1, 153.8, 148.5, 147.5, 142, 134.5, 132.5, 130.35, 130.3, 130.15, 129.9, 129.55, 129.1, 127.0, 125.2, 125.7, 122.7, 119.0, 111.8. ESI-MS [M+H$^+$]: m/z calcd for $C_{31}H_{20}N_4S$ 480.6, found 481.3.

4-(7-(4-Diphenylamino)phenyl)benzo[c][1,2,5]thiadiazol-4-yl)benzaldehyde (**3**).[41] Synthesized following the procedure similar to **1** with **1a** (1.0 g, 2.2 mmol, 1.0 eq), sodium carbonate (463 mg, 4.4 mmol, 2.0 eq), 4-formylphenylboronic acid (327 mg, 2.2 mmol, 1 eq), and tetrakis (triphenylphosphine) palladium (151 mg, 0.065 mmol, 0.1 eq). The product was purified over silica gel (hexane/dichloromethane; 40: 60%) to give a red solid (600 mg, 53%). ^{1}H NMR (400 MHz, $CDCl_3$) δ 10.15 (s, 1H), 8.21 (d, J=8.2 Hz, 2H), 8.09 (d, J=8.4 Hz, 2H), 7.96 – 7.87 (m, 3H), 7.83 (d, J=7.4 Hz, 1H), 7.34 (dd, J=11.1, 4.6 Hz, 4H), 7.24 (t, J=8.2 Hz, 6H), 7.12 (t, J=7.3 Hz, 2H). ^{13}C NMR ($CDCl_3$, 100 MHz) δ ppm=191.9, 154.1, 153.9, 148.5, 147.5, 143,5, 135.8, 134.2, 131.0, 130.4, 130.1, 130.0, 129.9, 129.5, 129.1, 127.1, 125.2, 123.6, 122.7. ESI-MS [M+H$^+$]: m/z calcd for $C_{31}H_{21}N_3OS$ 483.6, found 484.3.

N,*N*-Diphenyl-4-(7-phenylbenzo[c][1,2,5]thiadiazol-4-yl)aniline (**4**).[42] 4,7-Dibromobenzo[c][1,2,5]thiadiazole (600 mg, 1.31 mmol) and phenylboronic acid (240 mg, 1.965 mmol) were dissolved in a solution of 1,4-dioxane (30 mL). Aqueous Cs_2CO_3 (2 M, 2.0 mL) was then added and the mixture was bubbled with nitrogen for 15 min followed by the addition of tetrakis(triphenylphosphine)palladium(0) (76 mg, 0.0655 mmol). Nitrogen was bubbled again for 15 min. The mixture was stirred and heated at 100 ^{0}C overnight under a static nitrogen environment. After cooling the reaction mixture to room temperature, the crude product was extracted with dichloromethane (3×20 mL). The organic layer was dried over $MgSO_4$, filtered, and the solvent was evaporated. The crude product was then purified by silica gel chromatography using *n*-hexane/dichloromethane (5:1) as the eluent. The product was isolated as a yellow solid (350 mg, 59%). ^{1}H NMR (400 MHz, $CDCl_3$, δ): 7.97 (d, J=7.1 Hz, 1H), 7.88 (d, J=8.7 Hz, 1H), 7.79 – 7.75 (m, 1H), 7.55 (t, J=7.6 Hz, 1H), 7.46 (t, J=7.4 Hz, 1H), 7.33 – 7.28 (m, 2H), 7.21 (m, 3H), 7.07 (t, J=7.3 Hz, 1H). HRMS [M+H$^+$]: m/z calcd for $C_{30}H_{21}N_3S$ 456.1529, found 456.1523.

The spectroscopic, fluorescence, emission yields, spectroelectrochemical, and electrochemical measurements were done as previously reported.[43] For the solid-state emission, the given sample was coated on either a glass microscope coverslip or a rectangular 60 μL well quartz slide with a matching straight quartz plate. The emission yields were measured with an integrating sphere using either a pristine coverslip or an empty rectangular 60 μL well quartz slide as the reference substrate for measuring the scattering according to the direct and indirect methods.[44] Oxygen-free Φ_{fl} measurements of the fluorophore in the solid state were done by placing the fluorophore coated coverslip in a polyethylene pouch. The bag was evacuated and then heat sealed. Any emission of the plastic wrapping was eliminated from the measurements by measuring a blank pristine coverslip that was prepared under similar vacuum sealing conditions. Background emission of the plastic wrapped blank coverslip was minimal and it occurred in the UV region that was outside the spectral window used for the fluorophore measurements. The Φ_{fl} of the devices was measured with an integrating sphere using devices without the fluorophore as the reference.

The spectroelectrochemistry in solution was measured with a 1.8 mm optical path quartz cuvette. A 1.7 mm ceramic honeycomb gold electrode with 19-well electrodes was used as the working electrode with embedded gold counter and gold reference electrodes. The redox potentials measured with the gold honeycomb electrode could be converted to the potentials measured by cyclic voltammetry with an equimolar Fc/Fc$^+$ internal reference vs SCE by applying a −50 mV conversion factor. Similarly, the conversion factor for the redox potentials measured with the silver wire pseudo reference to SCE was 60 mV at the concentration used for the spectroscopic measurements. The electrofluorescence in solution was measured in a 0.5 mm optically narrow quartz cell with a 0.5 mm thick platinum gauze working electrode (7 mm x 5 mm), a platinum wire counter electrode, and a silver wire pseudo-electrode. The cuvette was oriented at 45° to the incident light for monitoring the emission. The dual-mode electrochromic/electrofluorochromic device was prepared by spray coating the given fluorophore on a square (25 x 25 mm) ITO coated glass slide (slide A). A stock solution of PMMA (5 g; MW~120 000 g/mol) was dissolved in dichloromethane (10 mL) along with lithium perchlorate (300 mg, 2.82 mmol) and propylene carbonate (8 g) to give a transparent gel.[45] The gel was stirred overnight and it was drop cast on a different ITO glass slide (slide B). Both ITO substrates (Slides A+B) were then sandwiched together with the intrinsic thickness of the electrolyte layer acting as the spacer. Copper tape was fixed to each electrode for the electrochromic/electrofluorochromic studies. The coloration efficiency (η) was calculated from the change in absorbance between the colored and bleached states over the integrated chronoamperometry per the known area of the working device in both solution and devices. The color contrast ratio was taken as the difference between transmission % of the bleached and colored states over the transmission percent of the bleached state. The fluorescence contrast ratio was similarly calculated according to the integrated areas of the corresponding emission spectra. The coloration kinetics were fitted to first order growth and decay fits similar to known means.[35]

Theoretical calculations were done with Gaussian Rev. 16 C.01[46] using the CAM–B3LYP[47] functional along with the 6–311 G+(d,p) basis set along with the Grimme D3 empirical dispersion.[48] All the frequencies of the ground state optimized structures of the fluorophores in their various charges (neutral and radical cation) were positive. Dichloromethane was used as the solvent continuum (IEFPCM) for all the calculations. This same level of theory, functional, and the basis set were used to calculate the various states according by corrected linear response method.[49] In short, the ground state was first optimized, followed by the unequilibrated solvated TD-DFT calculations of the first 5 excited states to give the electronic absorption transitions. This was then used to calculated the optimized geometry of the excited state also by TD-DFT. The principal highest occupied and lowest unoccupied orbitals involved in the lowest energy electronic transition were calculated from the Natural Transition Orbitals (NTOs).[50] The NTOs were used for visual purposes (Figure S24). Restricted open Hartree-Fock was used to calculate the ground state geometry and the corresponding electron spin distribution of the open-shelled intermediates. Unrestricted Hartree-Fock as used for the TD-DFT calculations and the corresponding NTOs wile restricted Hartree-Fock was used for the closed shelled systems.

Acknowledgements

The Natural Sciences and Engineering Council Canada and the Canada Foundation for Innovation are acknowledged for operating and infrastructure grants that enabled this work. C.Y. expresses thanks to MITACS, UdeM, and J. & M. Lemay for a Globalink undergraduate and graduate awards that supported

this work. G.B.M. also acknowledges Mitacs for a Globalink scholarship. C.C. thanks the French regional government for a travel award for undertaking the spectroscopic studies. The Quebec Center for Advanced Materials, formerly CSACS, is also acknowledged for access to equipment. The Digital Alliance of Canada, formally Compute Canada (www.computecanada.ca) and their partners, Compute Ontario (computeontario.ca) and WestGrid (www.westgrid.ca), are also thanked for access to both computational resources and software for theoretical calculations. L. Walach and G. Turner are also thanked for preliminary spectroscopic studies and electrochromic measurements.

Conflict of Interests

The authors declare no conflict of interest.

Data Availability Statement

The data that support the findings of this study are available from the corresponding author upon reasonable request.

Keywords: fluorescence · electrochromism · electrofluorochromism · reversible oxidation · reversible color change

[1] M. H. Chua, T. Tang, K. H. Ong, W. T. Neo, J. W. Xu in *Chapter 1: Introduction to Electrochromism*, Eds.: J. W. Xu, M. H. Chua and K. W. Shah, The Royal Society of Chemistry, **2019**, 1–21.
[2] a) C. G. Granqvist, *Thin Solid Films* **2014**, *564*, 1–38; b) J. L. R. Warner, S. E. M. S.Selkowitz, D. K. Arasteh in *Utility and Economic Benefits of Electrochromic Smart Windows*, *Vol.* Lawrence Berkeley National Laboratory, **1992**.
[3] a) D. Ma, J. Wang, *Sci. China Chem.* **2017**, *60*, 54–62; b) S. Cong, F. Geng, Z. Zhao, *Adv. Mater.* **2016**, *28*, 10518–10528
[4] a) J. A. Kerszulis, K. E. Johnson, M. Kuepfert, D. Khoshabo, A. L. Dyer, J. R. Reynolds, *J. Mater. Chem. C* **2015**, *3*, 3211–3218; b) P. M. Beaujuge, S. Ellinger, J. R. Reynolds, *Nat. Mater.* **2008**, *7*, 795–799; c) A. L. Dyer, E. J. Thompson, J. R. Reynolds, *ACS Appl. Mater. Interfaces* **2011**, *3*, 1787–1795.
[5] a) P. Audebert, F. Miomandre, *Chem. Sci.* **2013**, *4*, 575–584; b) I. Seddiki, B. I. N'Diaye, W. G. Skene, *Molecules* **2023**, *28*, 3225; c) G. A. Corrente, A. Beneduci, *Adv. Opt. Mater.* **2020**, *8*, 2000887; d) K. Nakamura, K. Kanazawa, N. Kobayashi, *J. Photochem. Photobiol. A* **2022**, *50*, 100486.
[6] a) K. Muras, M. Kubicki, M. Wałęsa-Chorab, *Dyes and Pigments* **2023**, *212*, 111098; b) S. Halder, S. Pal, P. Sivasakthi, P. K. Samanta, C. Chakraborty, *Macromolecules* **2023**, *56*, 2319–2327; c) C. Quinton, V. Alain-Rizzo, C. Dumas-Verdes, G. Clavier, F. Miomandre, P. Audebert, *European Journal of Organic Chemistry* **2012**, *2012*, 1394–1403; d) C. Quinton, V. Alain-Rizzo, C. Dumas-Verdes, F. Miomandre, G. Clavier, P. Audebert, *RSC Adv.* **2014**, *4*, 34332–34342; e) C. Quinton, V. Alain-Rizzo, C. Dumas-Verdes, F. Miomandre, G. Clavier, P. Audebert, *Chem. Eur. J.* **2015**, *21*, 2230–2240
[7] M. R. Anthony Raj, C. Yao, M. Frémont, W. G. Skene, *Chemistry – A European Journal* **2024**, *30*, e202401417.
[8] a) J.-L. Wang, Q. Xiao, J. Pei, *Org. Lett.* **2010**, *12*, 4164–4167; b) J. E. Barnsley, G. E. Shillito, J. I. Mapley, C. B. Larsen, N. T. Lucas, K. C. Gordon, *J. Phys. Chem. A* **2018**, *122*, 7991–8006; c) R. Misra, P. Gautam, *Org. Biomol. Chem.* **2014**, *12*, 5448–5457; d) A. Pathak, T. Tomer, K. J. Thomas, M.-S. Fan, K.-C. Ho, *Electrochim. Acta* **2019**, *304*, 1–10.
[9] a) X. Wang, K. Wang, M. Wang, *Polym. Chem.* **2015**, *6*, 1846–1855; b) J. Zhang, T. C. Parker, W. Chen, L. Williams, V. N. Khrustalev, E. V. Jucov, S. Barlow, T. V. Timofeeva, S. R. Marder, *J. Org. Chem.* **2015**, *81*, 360–370
[10] a) T. Ishi-i, H. Tanaka, R. Youfu, N. Aizawa, T. Yasuda, S.-i. Kato, T. Matsumoto, *New J. Chem.* **2019**, *43*, 4998–5010; b) Z. Peng, Z. Wang, Z. Huang, S. Liu, P. Lu, Y. Wang, *J. Mater. Chem. C* **2018**, *6*, 7864–7873; c) M. Wałęsa-Chorab, S. F. Ekti, M. Simard, W. G. Skene, *J. Mol. Struct.* **2024**, *1314*, 138637.
[11] K. Balakrishnan, W.-L. Hsu, S. Mataka, S. Pau, *Chem. Commun.* **2014**, *50*, 5600–5603.
[12] a) M. Wałęsa-Chorab, M.-H. Tremblay, M. Ettaoussi, W. G. Skene, *Pure Appl. Chem.* **2016**, *87*, 649–661; b) A. Pazini, L. Maqueira, F. D. Santos, A. R. J. Barreto, R. D. Carvalho, F. M. Valente, D. Back, R. Q. Aucelio, M. Cremona, F. S. Rodembusch, J. Limberger, *Dyes Pigm.* **2020**, *178*, 108377.
[13] B. A. D. Neto, P. H. P. R. Carvalho, J. R. Correa, *Acc. Chem. Res.* **2015**, *48*, 1560–1569.
[14] a) V. H. K. Fell, N. J. Findlay, B. Breig, C. Forbes, A. R. Inigo, J. Cameron, A. L. Kanibolotsky, P. J. Skabara, *J. Mater. Chem. C* **2019**, *7*, 3934–3944; b) S.-Y. Yang, Y.-L. Zhang, A. Khan, Y.-J. Yu, S. Kumar, Z.-Q. Jiang, L.-S. Liao, *J. Mater. Chem. C* **2020**, *8*, 3079–3087.
[15] W. Wu, Y. Yang, Y. Yang, Y. Yang, K. Zhang, L. Guo, H. Ge, X. Chen, J. Liu, H. Feng, *Small* **2019**, *15*, 1805549.
[16] Z. Li, W. Qin, J. Wu, Z. Yang, Z. Chi, G. Liang, *Mater. Chem. Front.* **2019**, *3*, 2051–2057.
[17] M. Mamada, R. Komatsu, C. Adachi, *ACS Appl. Mater. Interfaces* **2020**, *12*, 28383–28391.
[18] a) Y. Li, W. Wang, Z. Zhuang, Z. Wang, G. Lin, P. Shen, S. Chen, Z. Zhao, B. Z. Tang, *J. Mater. Chem. C* **2018**, *6*, 5900–5907; b) X. Chen, Z. Yang, W. Li, Z. Mao, J. Zhao, Y. Zhang, Y.-C. Wu, S. Jiao, Y. Liu, Z. Chi, *ACS Appl. Mater. Interfaces* **2019**, *11*, 39026–39034.
[19] K. R. Justin Thomas, J. T. Lin, M. Velusamy, Y.-T. Tao, C.-H. Chuen, *Adv. Funct. Mater.* **2004**, *14*, 83–90.
[20] A. Pathak, K. R. Justin Thomas, M. Singh, J.-H. Jou, *J. Org. Chem.* **2017**, *82*, 11512–11523.
[21] G. A. Corrente, D. A. González, E. Aktas, A. L. Capodilupo, G. Mazzone, F. Ruighi, G. Accorsi, D. Imbardelli, C. Rodriguez-Seco, E. Martinez-Ferrero, E. Palomares, A. Beneduci, *Adv. Opt. Mater.* **2022**, *11*, 2201506.
[22] a) M. Wałęsa-Chorab, W. G. Skene, *ACS Appl. Mater. Interfaces* **2017**, *9*, 21524–21531; b) T. Ghosh, S. Kandpal, C. Rani, L. Bansal, R. Kumar, *ACS Applied Optical Materials* **2023**, *1*, 915–923.
[23] C. G. Granqvist, *Solid State Ion.* **1992**, *53–56*, 479–489.
[24] J. R. Lakowicz, *Principles of Fluorescence Spectroscopy*, Springer, New York **2006**, 954.
[25] a) E. Lippert, *Zeitschrift für Elektrochemie, Berichte der Bunsengesellschaft für physikalische Chemie* **1957**, *61*, 962–975; b) N. Mataga, Y. Kaifu, M. Koizumi, *Bull. Chem. Soc. Jpn.* **2006**, *29*, 465–470.
[26] C. J. Seliskar, L. Brand, *J. Am. Chem. Soc.* **1971**, *93*, 5414–5420.
[27] a) P. Thamaraiselvi, E. Varathan, V. Subramanian, S. Easwaramoorthi, *Dyes Pigm.* **2020**, *172*, 107838; b) W. Li, Y. Pan, L. Yao, H. Liu, S. Zhang, C. Wang, F. Shen, P. Lu, B. Yang, Y. Ma, *Adv. Opt. Mater.* **2014**, *2*, 892–901.
[28] N. Katsumi, *Bull. Chem. Soc. Jpn.* **1982**, *55*, 2697–2705.
[29] J. Jortner, *Pure Appl. Chem.* **1971**, *27*, 389–419.
[30] Q. Ji, C. Chao, D. Dan, T. B. Zhong, *Adv. Healthcare Mater.* **2018**, *0*, 1800477.
[31] X. Shi, S. H. P. Sung, M. M. S. Lee, R. T. K. Kwok, H. H. Y. Sung, H. Liu, J. W. Y. Lam, I. D. Williams, B. Liu, B. Z. Tang, *J. Mater. Chem. B* **2020**, *8*, 1516–1523.
[32] M.-C. Chen, D.-G. Chen, P.-T. Chou, *ChemPlusChem* **2021**, *86*, 11–27.
[33] H.-J. Yen, G.-S. Liou, *Polym. Chem.* **2018**, *9*, 3001–3018.
[34] a) C. Lambert, G. Nöll, *J. Am. Chem. Soc.* **1999**, *121*, 8434–8442; b) F. Ruighi, E. Fabiano, L. Franco, A. Agostini, S. Zatta, G. A. Corrente, A. Beneduci, A. Cardone, G. Accorsi, A. L. Capodilupo, *Dyes Pigm.* **2023**, *219*, 111582.
[35] S. Hassab, D. E. Shen, A. M. Österholm, M. Da Rocha, G. Song, Y. Alesanco, A. Viñuales, A. Rougier, J. R. Reynolds, J. Padilla, *Sol. Energy Mater. Sol. Cells* **2018**, *185*, 54–60.
[36] M. R. A. Raj, C. Yao, M. Frémont, W. G. Skene, *Chem. Eur. J.* **2024**, *30*, e202401417.
[37] a) Y. Sun, M. Shi, Y. N. Zhu, I. F. Perepichka, X. Xing, Y. M. Liu, C. Y. Yan, H. Meng, *ACS Appl. Mater. Interfaces* **2020**, *12*, 24156–24164; b) G. K. Pande, D. Y. Kim, F. Sun, R. Pal, J. S. Park, *Sol. Energy Mater. Sol. Cells* **2023**, *263*, 112579; c) Y. Zhou, Z. Wang, Y. Ke, J. Zheng, C. Xu, *Dyes Pigm.* **2023**, *219*, 111620.
[38] N. Tsierkezos, *J. Solution Chem.* **2007**, *36*, 289–302.
[39] Y.-J. Shao, M.-H. Tu, G.-S. Liou, *Chem. Eng. J.* **2023**, *466*, 143003.
[40] P. Dutta, W. Yang, S. H. Eom, W.-H. Lee, I. N. Kang, *Chem. Commun.* **2012**, *48*, 573–575.

[41] J. Su, T. Fukaminato, J.-P. Placial, T. Onodera, R. Suzuki, H. Oikawa, A. Brosseau, F. Brisset, R. Pansu, K. Nakatani, R. Métivier, *Angew. Chem., Int. Ed.* **2016**, *55*, 3662–3666.
[42] W. Li, Q. Huang, Z. Mao, Q. Li, L. Jiang, Z. Xie, R. Xu, Z. Yang, J. Zhao, T. Yu, Y. Zhang, M. P. Aldred, Z. Chi, *Angew. Chem., Int. Ed.* **2018**, *57*, 12727–12732.
[43] M. Wałęsa-Chorab, C. Yao, G. Tuner, W. G. Skene, *Chem. Eur. J.* **2020**, *26*, 17416–17427.
[44] S. Leyre, E. Coutino-Gonzalez, J. J. Joos, J. Ryckaert, Y. Meuret, D. Poelman, P. F. Smet, G. Durinck, J. Hofkens, G. Deconinck, P. Hanselaer, *Rev. Sci. Instrum.* **2014**, *85*, 123115–123119.
[45] J.-H. Wu, G.-S. Liou, *Adv. Funct. Mater.* **2014**, *24*, 6422–6429.
[46] M. J. Frisch, G. W. Trucks, H. B. Schlegel, G. E. Scuseria, M. A. Robb, J. R. Cheeseman, G. Scalmani, V. Barone, G. A. Petersson, H. Nakatsuji, X. Li, M. Caricato, A. V. Marenich, J. Bloino, B. G. Janesko, R. Gomperts, B. Mennucci, H. P. Hratchian, J. V. Ortiz, A. F. Izmaylov, J. L. Sonnenberg, Williams, F. Ding, F. Lipparini, F. Egidi, J. Goings, B. Peng, A. Petrone, T. Henderson, D. Ranasinghe, V. G. Zakrzewski, J. Gao, N. Rega, G. Zheng, W. Liang, M. Hada, M. Ehara, K. Toyota, R. Fukuda, J. Hasegawa, M. Ishida, T. Nakajima, Y. Honda, O. Kitao, H. Nakai, T. Vreven, K. Throssell, J. A. Montgomery Jr., J. E. Peralta, F. Ogliaro, M. J. Bearpark, J. J. Heyd, E. N. Brothers, K. N. Kudin, V. N. Staroverov, T. A. Keith, R. Kobayashi, J. Normand, K. Raghavachari, A. P. Rendell, J. C. Burant, S. S. Iyengar, J. Tomasi, M. Cossi, J. M. Millam, M. Klene, C. Adamo, R. Cammi, J. W. Ochterski, R. L. Martin, K. Morokuma, O. Farkas, J. B. Foresman, D. J. Fox, *Gaussian 16 Rev. C.01*, Wallingford, CT, **2016**.
[47] M. J. G. Peach, E. I. Tellgren, P. Sałek, T. Helgaker, D. J. Tozer, *J. Phys. Chem. A.* **2007**, *111*, 11930–11935.
[48] S. Grimme, J. Antony, S. Ehrlich, H. Krieg, *J. Chem. Phys.* **2010**, *132*, 154104.
[49] C. Guido, S. Caprasecca, *How to perform corrected Linear Response calculations in G09* **2016**.
[50] R. L. Martin, *J. Chem. Phys.* **2003**, *118*, 4775–4777.

Manuscript received: October 26, 2024
Revised manuscript received: November 19, 2024
Accepted manuscript online: November 20, 2024
Version of record online: December 18, 2024